Indirect Magnetic Coupling in Light-Element-Doped Single-Walled Carbon Nanotubes

Vojislav Krstić,[†,*] Christopher P. Ewels,[‡,*] Thomas Wågberg,[§] Mauro S. Ferreira,[†] Anne M. Janssens,[∥] Odile Stéphan,[⊥] and Marianne Glerup[¶]

[†]School of Physics, Centre for Research on Adaptive Nanostructures and Nanodevices, Trinity College Dublin, College Green, Dublin 2, Ireland, [‡]Institut des Matériaux Jean Rouxel (IMN), CNRS, Université de Nantes, BP32229 Nantes, France, [§]Department of Physics, University of Umeå, 901 87 Umeå, Sweden, [∥]Kavli Institute of NanoScience, Delft University of Technology, P.O. Box 5046, 2600 GA, Delft, The Netherlands, [⊥]LPS, CNRS8502, Université Paris-Sud, Bat. 510, 91405 Orsay Cedex, France, and [¶]Department of Chemistry, University of Oslo, P.O. Box 1033, Blindern, 0315 Oslo, Norway

ABSTRACT Single-walled carbon nanotubes substitutionally doped with the light-element phosphorus are synthesized and are investigated by electrical and nuclear magnetic resonance measurements. Decreased spin—lattice relaxation times compared to undoped tubes point toward enhanced spin-sensitive scattering. Temperature dependence of the zero-bias conductance shows step-like features, a signature of scattering from a very low density (few sites per nanotube) of localized spin moments at oxidized phosphorus sites, consistent with density functional calculations. This supports recent predictions that localized magnetic moments must be indirectly magnetically coupled through the nanotube conduction electrons.

KEYWORDS: doped nanocarbon · magnetism · transport · NMR · spintronics · DFT

While discrete coupling between isolated magnetic moments has long been a playground for theoretical modeling, it has yet to be observed experimentally in individual carbon nano-objects. Isolated transition metal atom impurity doping of surfaces is difficult due to the high reactivity and tendency of such species to aggregate, and d^0 magnetism in doped carbon has not been reliably characterized. Thus, to date, no substitutional doping during synthesis leading to magnetic-moment-carrying sites has been achieved in doped carbon. Nonetheless, efficient and controlled tuning of the electronic and spin properties of carbon nanotubes is a key requirement for the application of this unique material for molecular-based nanoelectronics and spintronics.

Tailoring the electronic properties of carbon nanotubes (CNTs) *via* (substitutional) doping with boron or nitrogen has generated great interest,[1−5] and transport studies on doped single-walled[6,7] and multiwalled CNTs[8−10] have been reported. Regarding molecular spintronics, experimental and theoretical work on carbon-based nanomaterials[11−16] report on the formation of localized magnetic moments when substitutionally doped with transition metal atoms. Specific for CNTs, the same doping predicts long-range indirect exchange coupling[14−16] with significant impact on the transport properties[17] of the CNTs. However, the deliberate synthesis of CNTs with substitutional magnetic-moment-carrying atoms has not been achieved to the best of our knowledge.

In the present work, we demonstrate experimentally and theoretically that substitutional doping of single-walled carbon nanotubes (SWNTs) with nonmagnetic phosphorus bridges the gap between tailoring electrical transport and the spin-transport properties of SWNTs and provides novel insight into potential mechanisms toward d^0 magnetism[18−21] in organic materials.

RESULTS AND DISCUSSION

In all of our synthesis experiments (see Methods), the resultant so-called "collarets" (tube-rich deposits) around the cathode had the same structural characteristics as equivalent undoped samples, but the size of the collaret was significantly smaller. Scanning and transmission electron microscopy (SEM and TEM) images of ethanol-dispersed nanotubes without prior treatment were taken for the evaluation of homogeneity, purity, and structure of the material (Figure 1).

A typical SEM image shows a reasonably homogeneous complex of nanotube bundles (Figure 1a) with low content of

*Address correspondence to krsticv@tcd.ie, chris.ewels@cnrs-imn.fr.

Received for review April 27, 2010 and accepted July 29, 2010.

Published online August 4, 2010. 10.1021/nn1009038

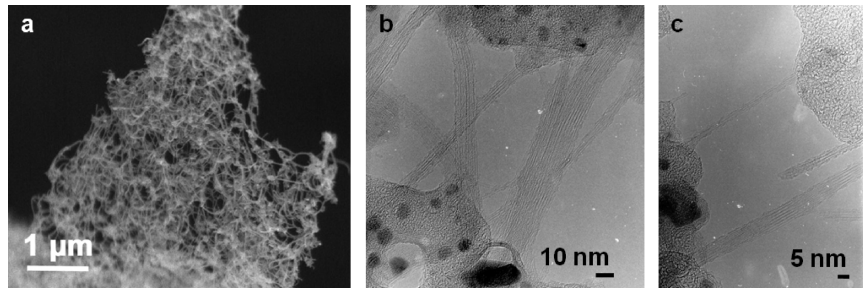

Figure 1. (a) Representative SEM image of the phosphorus-doped SWNTs. (b,c) TEM images of the phosphorus-doped SWNTs including abruptly ending tubes. The average diameter of the SWNTs is approximately 1.3 nm. Tubes were typically in bundles containing 10 to 20 nanotubes.

other carbon structures, such as graphite and fibers. TEM images (Figure 1b,c) show that the spongy collarets of both samples contain a high concentration of SWNT bundles, amorphous carbon, and encapsulated metal particles. However, a significant number of abruptly ending tubes were observed (Figure 1c). Electron energy loss spectroscopy on individual tubes revealed no evidence for any clustering of phosphorus atoms, at the same time allowing us to estimate that the phosphorus dopant concentration is well below 0.5 atom % (resolution limit).

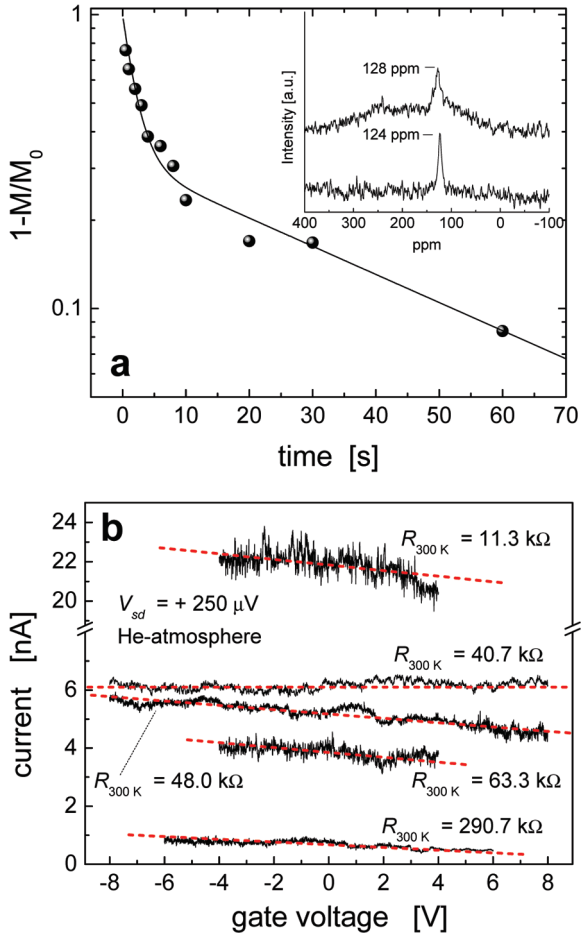

Figure 2. (a) Filled squares show $1-M/M_0$ of the phosphorus-doped sample plotted against recovery time ($M_0 = M_m + M_s$). The solid line is the data fitted to eq 1. Inset: ^{13}C NMR spectra of phosphorus-doped (top) and pristine SWNTs (bottom). The repetition time was 3 s for the phosphorus-doped and 20 s for the pure SWNT sample. (b) Electric field effect measurements on a number of phosphorus-doped SWNTs at room temperature. Diameters (nm) from top: 1.3, 1.1, 1.4, 1.1, 1.2. Only weak responses (or none, see middle line) to the applied gate voltage are observed, indicating that these tubes are metallic. The curves have a negative slope (red dashed lines are a guide to the eye), which is the signature of p-type conduction.

In Figure 2a, the magnetization saturation recovery curve ($1-M/M_0$ *versus* recovery time) for the synthesized phosphorus-doped nanotube sample is shown. M is the magnetization of the ^{13}C nuclei at time t, and M_0 is the magnetization at saturation which is assumed to be the sum of the magnetization M_m and M_s of metallic and semiconducting tubes,[22,23] respectively. The inset in Figure 2a shows the ^{13}C NMR MAS spectrum of the phosphorus-doped SWNTs together with a reference SWNT spectrum (reference tubes produced under identical conditions as the doped SWNTs). A paramagnetic shift of 4 ppm is seen, analogous to the paramagnetic shifts (~10 ppm) already observed in both alkaline metals and iodine intercalated SWNTs.[24]

The magnetization saturation recovery curve can be fitted using a double-exponential expression for the total magnetization

$$M = M_m[1 - \exp(-t/T_{1m})] + M_s[1 - \exp(-t/T_{1s})] \quad (1)$$

where T_{1m} and T_{1s} are the spin−lattice relaxation times for metallic and semiconducting SWNTs, respectively. The fit is in very good agreement with the experimental data and reveals a fast relaxing component $T_{1m} = 2.1 \pm 0.4$ s and a slow relaxing component $T_{1s} = 45 \pm 9$ s.

Strikingly, the relaxation times are significantly shorter than for undoped tubes for which $T_{1m} \approx 5$ s and $T_{1s} \approx 90$ s have been reported by several groups using the same method.[22,23] This reduction in relaxation time in the phosphorus-doped SWNTs implies the presence of an additional spin-sensitive scattering mechanism arising from phosphorus defects in the nanotube lattice.

From the magnitude of $M_m = 180 \pm 11$ emu and $M_s = 88 \pm 6$ emu, it can be deduced that the sample contains around 70% of the fast and 30% of the slow relaxing type. In contrast, for undoped SWNTs, approximately 33 and 67% were reported for M_m and M_s,

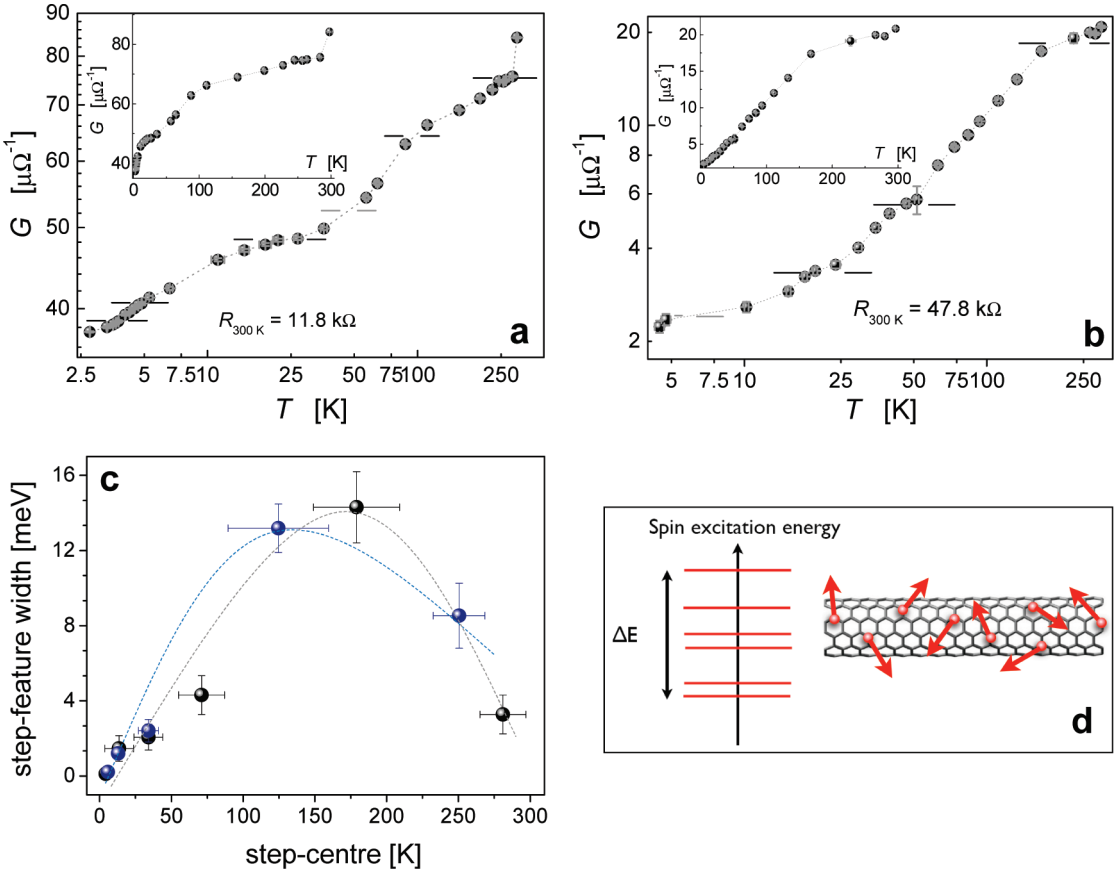

Figure 3. (a,b) Zero-bias conductance *G versus* temperature for two different phosphorus-doped SWNTs plotted in a double-logarithmic scale. For both, a nonlinear temperature dependence is observed with step-like features whose positions are denoted by short horizontal black lines (less clearer step features are denoted by gray lines), though differing in temperature step size. Insets: Zero-bias conductance *vs* temperature with linear scale axis. (c) Width of the step-like features in energy as a function of their position (center of the feature). For both samples (a, black; b, blue), the distribution in energies lies in the range of 0.5 to 15 meV. Lines are a guide to the eye. (d) Schematic SWNT doped with a few oxidized P atoms. Arrows represent randomly distributed and oriented magnetic moments associated with each P atom. The interaction between magnetic moments is mediated by the conduction electrons, known to generate long-ranged Heisenberg-like couplings. A small number of moments randomly dispersed within a nanotube leads to a discrete spin excitation spectrum (left panel). The magnitude of the energy dispersion, ΔE, reflects the characteristic values of the individual magnetic couplings.

respectively.[22,23] Thus, the concentration ratio of the fast and slow component implies that the presence of phosphorus during synthesis preferentially encourages metallic SWNT growth. We note that the observation of reduced relaxation time and the paramagnetic shift are strong indications for a successful phosphorus doping of the tubes.

The electrical transport has been probed on several individual (metallic) SWNTs at room temperature and down to 2.7 K. Metallic tubes have been chosen to circumvent Schottky-barrier-like effects. The measurements at room temperature on several individual phosphorus-doped SWNTs (Figure 2b) show weak (or no) electric field effect, which is the signature for metallic CNTs. More importantly, all measurements exhibit predominantly p-type conduction, which is in contrast to the naively expected n-type conduction for phosphorus atoms incorporated into a carbon nanotube lattice. At room temperature, the resistances are still comparable to values of undoped SWNTs, implying ballistic conduction within the distances defined by our electrode spacing of 200 nm (see Methods section), in agreement with the experimentally estimated low phosphorus dopant content.

In Figure 3a,b, the temperature dependence of the zero-bias conductance, G, of two individual phosphorus-doped SWNTs is plotted in a double-logarithmic scale. Strong nonlinear behavior is observed. In addition, step-like features are present which indicate that a second temperature-dependent process is active. For comparison, pristine SWNTs are known to exhibit Luttinger liquid-type behavior following the power law, $G(T) \sim T^{\gamma}$, with γ being a measure for the interaction strength between the conduction electrons.[25,26] In this case, a double-logarithmic plot of the zero-bias conductance *versus* temperature would yield a straight line. Clearly, this scenario does not coincide with the experimental results. Instead, the phosphorus-doped SWNTs must be regarded as disordered nanowires.[6] We note here that the combined results of our experimental NMR and electrical transport measurements provide unambiguous proof for the suc-

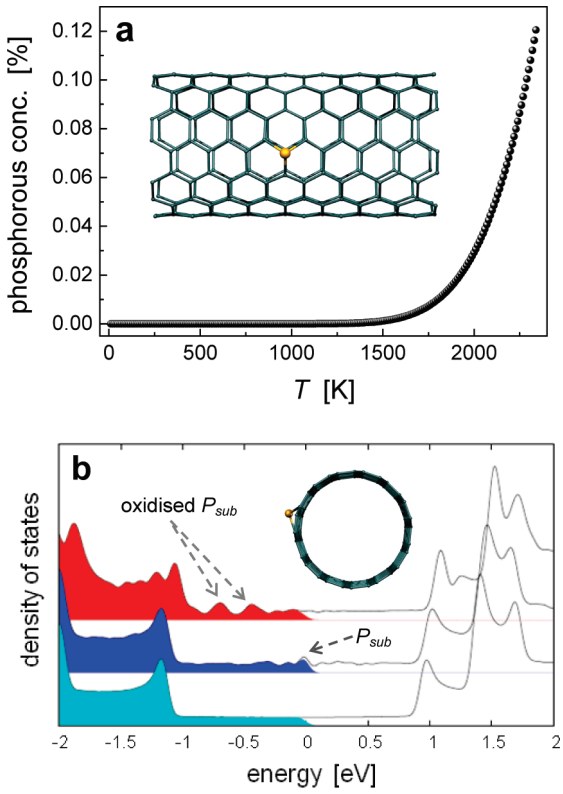

Figure 4. (a) Calculated thermodynamic equilibrium concentration of substitutional phosphorus (P_{sub}) in a (7,7) SWNT carbon lattice as a function of temperature (logarithmic scale). From about 1900 K and above, a measurable phosphorus content is expected. Inset: Side view of a P_{sub} center. (b) Density of states for an undoped (bottom), P_{sub} doped (center), and oxidized P_{sub} (top) doped (7,7) tube. The shaded area denotes filled states. Inset: View along the tube (7,7) axis with a P_{sub} center (formation energy 1.5 eV). The phosphorus shifts out of the nanotube surface plane by 1.3 Å, with bond lengths of 1.75 Å.

cessful phosphorus doping of our SWNTs in the low dopant concentration limit.

Insight into microscopic mechanisms was obtained by the modeling of the behavior of substitutional phosphorus (P_{sub}) defects in SWNTs[27,28] through a density functional approach: Due to its large radius, the phosphorus sits out of plane (inset Figure 4a,b) unlike nitrogen, with carbon−phosphorus bonds about 30% longer than standard carbon−carbon bonds.

From the calculated formation energy (1.5 eV), we obtain the thermal equilibrium point defect concentration of P_{sub} impurities in a metallic (7,7) SWNT as a function of temperature (Figure 4a), which is directly proportional to the probability of incorporation of phosphorus atoms. This shows that there should be phosphorus incorporation at temperatures above 1900 K, which is in agreement with studies of carbon nanotube formation temperature by the arc-discharge method.[29] However, the concentrations of incorporated phosphorus (up to 0.1 atom %) are low compared to those achieved in nitrogen-doped SWNTs (up to 1 atom %).[2] This low P_{sub} concentration (as a rough illustration, at 0.1 atom %, approximately 20 P atoms would be found in a 200 nm long (7,7) tube) matches with our experimental observation of ballistic conduction over at least 200 nm at room temperature.

To clarify the measured temperature dependence of the conductance and the electric field effect measurements, we next determined how stable a P_{sub} defect is against oxygenation since phosphorus is known to be one of the most oxygenophilic elements. The calculations reveal that oxidization of P_{sub} is highly exothermic (3.3 eV), and thus substitutional phosphorus atoms will instantly oxidize in the presence of O_2, an effect reported for phosphorus-doped fullerenes.[30] The oxidation impact can be understood within a simple molecular orbital picture: P_{sub} uses three electrons in σ-bonds, one p_z-orbital in the π-cloud (as for carbon), leaving one additional electron that is donated to the π-system, hence the center is a net donor. However, once oxidized, the phosphorus now uses both the p_z and the additional electron in the P═O bond. Thus replacement of a carbon by P═O removes one p_z electron from the π-system, and the defect is a net acceptor. In Figure 4b, the density of states of an undoped, phosphorus-doped, and an oxidized phosphorus-doped (7,7) SWNT are shown. The transformation of the P_{sub} center from a donor into an acceptor state is observed, in agreement with the observed p-type conduction at room temperature.

The origin of the step-like features in the zero-bias conductance must be a temperature-dependent mechanism. Pure phonon charge carrier scattering can be excluded due to phonon freeze-out. It is well-known that the P═O bond has a permanent electric dipole moment (1.88 D for phosphorus monoxide),[31] which our modeling confirms. More strikingly, our calculations show that the oxidized P_{sub} also carries unpaired electron spin: The creation of a chemically stable electric dipole leads to the formation of a spin moment of 0.52 μ_B. The presence of a spin moment is in agreement with the shortening of the relaxation times T_{1m} and T_{1s} observed in the NMR experiment. Recent theoretical work predicts that two localized magnetic moments embedded in a nanotube may interact through the conduction electrons of the tube with a Heisenberg-like behavior, which forces the moments into a collinear alignment. Whether they prefer a parallel or antiparallel alignment depends primarily on their separation and specific sublattice site.[14−16] However, in the case considered here, where the oxidized P_{sub} atoms are randomly distributed within the nanotube, the magnetic alignment of each moment is the result of a competition between all of these pairwise interactions, which works against collinear arrangements of the moments. While the precise magnetic arrangement is difficult to predict due to the intrinsic randomness in their positions, one can certainly conclude that in the limit of low dopant concentration this interaction leads to a discrete spectrum in their spin excitations. An estimate for the energy

range ΔE of these excitations can be made by applying a one-dimensional spin-chain model,[32] which gives ΔE to be between 2 and 20 meV (Figure 3d). We used values for the total exchange interaction between the phosphene centers based on recent calculations on substituted magnetic-moment-carrying atoms.[13] In Figure 3c, the center of the step features and their width in millielectronvolts are depicted. For both tubes, a similar dependence is observed with maximum energies around 15 meV, in very good agreement with our energy estimation for the spin excitations. We emphasize that electric dipoles cannot account for the observed step-like features because of the much more rapid decay of the electric dipole interaction compared to the spin−spin interaction in a carbon nanotube.[33] Thus, in the limit of low concentrations, as in our material, spin−spin interaction will always dominate. More fundamentally, even if the electric dipoles were to generate some discrete energy levels, these would all be degenerate and thus cannot be the origin of a series of step-like features in the temperature dependence of the conductance.

Therefore, the experimental transport and NMR results, supported by our theoretical modeling, and in combination with previously reported spin considerations in CNTs,[14−17] underpin our reasoning that indeed the step-like features in the conductance are signatures of an indirect spin interaction between the phosphene centers in CNTs.

Recent studies of HOPG using magnetic force microscopy[21] elegantly showed that d^0 magnetism in pure multilayer carbon[21] can be explained *via* the presence of spin along grain boundaries. However, the current results cannot be explained in this way since single-walled nanotubes are seamlessly rolled up graphene lacking any grain boundaries. Thus, our results provide an alternative coupled point-defect-mediated mechanism for d^0 magnetism in d^0-doped graphitic carbon nanomaterials.

CONCLUSIONS

In summary, we probed the impact of phosphorus doping in single-walled carbon nanotubes using complementary techniques, nuclear magnetic resonance, and electrical measurements. NMR shows significantly reduced relaxation times, indicating enhanced charge carrier spin scattering. In addition, the magnetization−magnitude ratio for metallic and semiconducting phosphorus-doped nanotubes points toward encouraged metallic nanotube growth.

Electrical transport measurements on individual (metallic) nanotubes at room temperature and down to 2.7 K were performed. At room temperature, the electric field effect on metallic phosphorus-doped SWNTs shows p-type conduction. This agrees with our density functional calculations, which show that due to oxygen exposure the phosphorus centers form phosphene oxide centers which are electron acceptor sites. In addition, our calculations reveal the existence of a strong permanent electric dipole moment, which generates a localized spin moment at the phosphene oxide centers.

Zero-bias conductance measurements at varying temperature demonstrate that the incorporation of phosphorus converts the intrinsic transport properties of the nanotube to a disordered wire-type. Moreover, step-like features are observed in the zero-bias conductance, which are attributed to signatures of the indirect exchange coupling of the localized spin moments at the phosphene centers. Thus, this demonstrates that doping of single-walled carbon nanotubes with phosphorus overcomes the need for substitutional doping of magnetic-moment-carrying atoms for use in molecular spintronics.

METHODS

Synthesis of Phosphorus-Doped Single-Walled Carbon Nanotubes. While phosphorus-doped SWNTs have been recently reported using chemical vapor deposition,[34] our nanotubes were synthesized by arc-discharge (He atmosphere) using NiY catalyst, with phosphorus introduced to the anode rod by mixing graphite with red phosphorus.

For synthesis, the phosphorus content in the anode rod was varied to be either 1 or 2 atom %, by mixing 97.8 and 96.8 atom % graphite (1−2 μm, Aldrich) with 1 and 2 atom % red phosphorus (red P, 99%, Aldrich), respectively. In all experiments, 0.6 atom % Ni/0.6 atom % Y were used as the catalyst (Ni, 99.999%, ~100 mesh, Aldrich; Y, 99.9%, ~40 mesh, Aldrich). The solid mixtures were packed into the drillings of the anode rods. In an atmosphere of helium gas (660 mbar), an electrical current of approximately 100 A and 35 V was applied.

Nuclear Magnetic Resonance Measurements. To obtain information on the composition of the synthesized nanotube material, ^{13}C NMR experiments at room temperature were carried out. The magic-angle spinning (MAS) technique was used with a spin rate of 10 kHz to fully remove the side bands in the NMR spectra. For the experiments, 20 mg of highly nanotube-rich material, selected by X-ray analysis, was mixed with alumina powder to enable higher spin rates in the MAS measurements and to separate magnetic impurities. A spin rate of 10 kHz was chosen in all high-resolution experiments, which completely removed the side bands in the NMR spectra. As a reference, pure SWNTs were used, synthesized using the same method as our phosphorus-doped sample. The NMR experiments were performed using a Bruker ASX200 (50 MHz) at 4.7 T. The static ^{13}C spin−lattice relaxation experiments were performed on nanotube samples in evacuated glass tubes using a saturation recovery pulse technique and a Hahn echo as detection sequence. To obtain the spin relaxation times, T_1, and the magnitude of the magnetizations, M, the Levenberg−Marquardt algorithm (χ^2 minimization) was used.

Electrical Transport. For the electrical characterization of individual doped nanotubes, the tubes were first dispersed in solution and then deposited on a thermally grown SiO_2 layer on top of a highly doped Si wafer (serves as back-gate).[35] Single tubes were then contacted in a two-terminal configuration by standard electron-beam lithography, with AuPd as electrode material and an electrode distance of 200 nm; that is, the active conduction channel length of the tubes in all of our devices was defined

by this distance. The samples were investigated in helium atmosphere.

Theoretical Modeling. With respect to structural modeling, spin-unrestricted density functional calculations were performed using the local density approximation,[27,28] with a basis of localized Gaussian orbitals (22 Gians per C atom, 38 per P, 40 per O), using pseudopotentials to remove core electrons. Calculated tubes used 448 atom supercells. For formation energy calculations, standard states were taken as an isolated oxygen molecule (O_2), an isolated phosphorus tetrahedron (P_4), and carbon atoms from a pristine (7,7) carbon nanotube. This gave a vacancy formation energy of 7.4 eV, in good agreement with previous literature studies.[36,37]

Acknowledgment. V.K. acknowledges support from the Science Foundation Ireland (PI-award 08/IN.1/I1873). Parts of this work have been carried out within the NANOSIM_GRAPHENE project No. ANR-09-NANO-016-01 funded by the French National Agency (ANR) in the frame of its 2009 program in Nanosciences, Nanotechnologies & Nanosystems (P3N2009). C.P.E. and V.K. acknowledge support from the COST network MP0901, "NanoTP". The authors acknowledge helpful discussions with S. Sanvito.

REFERENCES AND NOTES

1. Terrones, M.; Jorio, A.; Endo, M.; Rao, A. M.; Kim, Y. A.; Hayashi, T.; Terrones, H.; Charlier, J. C.; Dresselhaus, G.; Dresselhaus, M. S. New Direction in Nanotube Science. *Mater. Today* **2004**, *10*, 30–45.
2. Ewels, C. P.; Glerup, M. Review of Nitrogen Doping in Carbon Nanotubes. *J. Nanosci. Nanotechnol.* **2005**, *5*, 1345.
3. Glerup, M.; Steinmetz, J.; Samaille, D.; Stéphan, O.; Enouz, S.; Loiseau, A.; Roth, S.; Bernier, P. Synthesis of N-Doped SWNT Using the Arc-Discharge Procedure. *Chem. Phys. Lett.* **2004**, *387*, 193–197.
4. Tang, C.; Bando, Y.; Goldberg, D.; Xu, F. Structure and Nitrogen Incorporation of Carbon Nanotubes Synthesized by Catalytic Pyrolysis of Dimethylformamide. *Carbon* **2004**, *42*, 2625–2633.
5. Gai, P. L.; Stéphan, O.; McGuire, K.; Rao, A. M.; Dresselhaus, M. S.; Dresselhaus, G.; Colliex, C. Structural Systematics in Boron-Doped Single Wall Carbon Nanotubes. *J. Mater. Chem.* **2004**, *14*, 669–675.
6. Krstić, V.; Rikken, G. L. J. A.; Bernier, P.; Roth, S.; Glerup, M. Nitrogen-Doping of Single-Walled Carbon Nanotubes: n-Type Conduction and Dipole Scattering. *Europhys. Lett.* **2007**, *77*, 37001-p1–37001-p5.
7. Krstić, V.; Glerup, M.; Hansel, S.; Lafkioti, M. Doped Single-Walled Carbon Nanotubes and Low-Mobility Graphene: Impact of Disorder and Dopants on Electronic Magnetotransport. *Phys. Status Solidi* **2009**, *3*, 187–189.
8. Choi, Y. M.; *et al.* Nonlinear Behavior in the Thermopower of Doped Carbon Nanotubes Due to Strong, Localized States. *Nano Lett.* **2003**, *3*, 839–842.
9. Krstić, V.; Blumentritt, S.; Muster, J.; Roth, S.; Rubio, A. Role of Disorder on Transport in Boron-Doped Multiwalled Carbon Nanotubes. *Phys. Rev. B* **2003**, *67*, 041401(R)-1–041401(R)-4.
10. Zhang, W. J.; Zhang, J. Y.; Li, P. L.; Shen, X.; Zhang, Q. F.; Wu, J. L. The Effects of Contacts and Ambipolar Electrical Transport in Nitrogen Doped Multiwall Carbon Nanotubes. *Nanotechnology* **2008**, *19*, 085202-1–085202-5.
11. Ushiro, M.; *et al.* X-ray Absorption Fine Structure (XAFS) Analysis of Ni Species Trapped in Graphene Sheet of Carbon Nanofibres. *Phys. Rev. B* **2006**, *73*, 144103-1–144103-11.
12. Santos, E. J. G.; *et al.* Switching on Magnetism in Ni Doped Graphene: Density Functional Calculations. *Phys. Rev. B* **2008**, *78*, 195420-1–195420-5.
13. Krasheninnikov, A. V.; Lehtinen, P. O.; Foster, A. S.; Pyykko, P.; Nieminen, R. M. Embedding Transition-Metal Atoms in Graphene: Structure Bonding, and Magnetism. *Phys. Rev. Lett.* **2009**, *102*, 126807-1–126807-4.
14. Costa, A. T.; Kirwan, D. F.; Ferreira, M. S. Indirect Exchange Coupling between Magnetic Adatoms in Carbon Nanotubes. *Phys. Rev. B* **2005**, *72*, 085402-1–085402-8.
15. Costa, A. T.; Rocha, C. G.; Ferreira, M. S. Noncollinear Coupling between Magnetic Adatoms in Carbon Nanotubes. *Phys. Rev. B* **2007**, *76*, 085401-1–085401-5.
16. Kirwan, D. F.; Rocha, C. G.; Costa, A. T.; Ferreira, M. S. Sudden Decay of Indirect Exchange Coupling between Magnetic Atoms on Carbon Nanotubes. *Phys. Rev. B* **2008**, *77*, 085432-1–085432-6.
17. Kirwan, D. F.; de Menezes, V. M.; Rocha, C. G.; Costa, A. T.; Muniz, R. B.; Fagan, S. B.; Ferreira, M. S. Enhanced Spin-Valve Effect in Magnetically Doped Carbon Nanotubes. *Carbon* **2009**, *47*, 2533–2537.
18. Coey, J. M. D. d^0 Ferromagnetism. *Solid State Sci.* **2005**, *7*, 660–667.
19. Droghetti, A.; Pemmaraju, C. D.; Sanvito, S. Predicting d^0 Magnetism: Self-Interaction Correction Scheme. *Phys. Rev. B* **2008**, *78*, 140404(R)-1–140404(R)-4.
20. For an overview on this topic refer to carbon-based magnetism, see: *An Overview of the Magnetism of Metal-Free Carbon-Based Compounds and Materials*; Makarova, T., Palacio, F., Eds.; Elsevier: Amsterdam, 2006.
21. Červenka, J.; Katsnelson, M. I.; Flipse, C. F. J. Room-Temperature Ferromagnetism in Graphite Driven by Two-Dimensional Networks of Point Defects. *Nat. Phys.* **2009**, *5*, 840–844.
22. Tang, X.-P.; et al. Electronic Structures of Single-Walled Carbon Nanotubes Determined by NMR. *Science* **2000**, *288*, 492–494.
23. Goze-Bac, C.; *et al.* Magnetic Interactions in Carbon Nanostructures. *Carbon* **2002**, *40*, 1825–1842.
24. Wågberg, T.; Goze-Bac, C.; Röding, R.; Sundqvist, B.; Johnels, D.; Kataura, H.; Bernier, P. 13C-NMR on Intercalated 2D-Polymerised C_{60} and Modified Peapods. In *Electronic Properties of Synthesized Nanostructures*, Proc. XVIII Int. Winterschool; Kuzmany, H., Fink, J., Mehring, M., Roth, S., Eds.; Melville: New York, 2004; pp 238−241.
25. Bockrath, M.; Cobden, D.; Liu, J.; Rinzler, A. G.; Smalley, R.; Balents, L.; McEuen, P. L. Luttinger-Liquid Behaviour in Carbon Nanotubes. *Nature* **1999**, *397*, 598–601.
26. For a review on Luttinger liquid behavior in carbon nanotubes, see: Egger, R.; Bachtold, A.; Fuhrer, M.; Bockrath, M.; Cobden, D.; McEuen, P. L. Luttinger Liquid Behaviour in Metallic Carbon Nanotubes. In *Interacting Electrons in Nanostructures*; Haug, R., Schoelle, H., Eds.; Springer: Berlin, 2002; pp 125−146, and references therein.
27. Jones, R.; Briddon, P. LDA Calculations Using a Basis of Gaussian Orbitals. *Phys. Status Solidi B* **2000**, *217*, 131–171.
28. Rayson, M. J.; Briddon, P. R. Rapid Iterative Method for Electronic-Structure Eigenproblems Using Localised Basis Functions. *Comput. Phys. Commun.* **2007**, *178*, 128–134.
29. Keidar, M. Factors Affecting Synthesis of Single-Walled Carbon Nanotubes in Arc Discharge. *J. Phys. D: Appl. Phys.* **2007**, *40*, 2388–2393.
30. Ewels, C. P.; El Cheikh, H.; Suarez-Martineza, I.; Van Lier, G. Oxidation and Reactivity of Nitrogen- and Phosphorus-Doped Heterofullerenes. *Phys. Chem. Chem. Phys.* **2008**, *10*, 2145–2148.
31. *CRC Handbook of Chemistry and Physics*, 84th ed.; Lide, D. R., Ed.; CRC Press LCC: Boca Raton, FL, 2003, pp 9−46.
32. Feymann, R. P. *Statistical Mechanics, A Set of Lectures*; Addison Wesley: New York, 1972; pp 198−220.
33. Jackson, J. D. *Classical Electrodynamics*, 3rd ed.; John Wiley & Sons Inc.: New York, 1999; pp 151−152.
34. Maciel, I. O.; *et al.* Synthesis, Electronic Structure, and Raman Scattering of Phosphorous-Doped Single-Walled Carbon Nanotubes. *Nano Lett.* **2009**, *9*, 2267–2272.
35. Krstić, V.; Roth, S.; Burghard, M. Phase Breaking in Three-Terminal Contacted Single-Walled Carbon Nanotube Bundles. *Phys. Rev. B* **2003**, *62*, R16353–R16355.
36. Thrower, P. A.; Mayer, R. M. Point Defects and Self-Diffusion in Graphite. *Phys. Status Solidi A* **1978**, *47*, 11–37.
37. El-Barbary, A. A.; Telling, R. H.; Ewels, C. P.; Heggie, M. I.; Briddon, P. R. Structure and Energetics of the Vacancy in Graphite. *Phys. Rev. B* **2003**, *68*, 144107-1–144107-7.